Available online at www.sciencedirect.com

ScienceDirect

Energy Procedia 44 (2014) 192 – 202

Energy Procedia

E-MRS Spring Meeting 2013 Symposium D - Advanced Inorganic Materials and Structures for Photovoltaics, 27-31 May 2013, Strasbourg, France

Equivalent-circuit and transport-based mobility models of microcrystalline silicon solar cells

Steve Reynolds[a,]*, Aad Gordijn[b], Vladimir Smirnov[b]

[a]*Division of Physics, University of Dundee, Small's Wynd, Dundee DD1 4HN, UK.*
[b]*IEK-5 Photovoltaik, Forschungszentrum Jülich, D-52425 Jülich, Germany*

Abstract

Microcrystalline silicon thin film solar cells exhibit optimal PV efficiency when the absorber layer contains similar proportions of crystalline and amorphous phases. When the crystalline fraction is reduced below 30%, efficiency falls very steeply, from around 8% to as low as 2%, and does not recover until fully amorphous growth conditions are established. We demonstrate that an electrical model, comprising two parallel-connected diodes scaled to reflect material composition, qualitatively predicts the features observed in the PV parameters. However the scale of the reduction in fill-factor is not reproduced. As an alternative approach, a homogeneous transport model is proposed in which carrier mobilities are scaled in accordance with values determined by the time-of-flight experiment. This model predicts a large reduction in fill-factor for low-crystallinity absorbers more in keeping with measurement. A novel carrier transport landscape is proposed to account for mobility variations.

Keywords: Microcrystalline silicon; solar cells; computer modelling; carrier transport; mobility

1. Introduction

The structural and optoelectronic properties of thin-film silicon may be controlled by the use of a process gas consisting of silane diluted in hydrogen. At silane concentrations $SC = [SiH_4]/([H_2] + [SiH_4])$ typically below 10% under VHF PECVD conditions, mixed-phase microcrystalline silicon of good optoelectronic quality, consisting of

* Corresponding author. Tel.: +44(0)1382 384559; fax: +44(0)1382 384389.
E-mail address: s.z.reynolds@dundee.ac.uk

doi:10.1016/j.egypro.2013.12.027

similar volumes of crystalline and amorphous material, may be deposited. By careful adjustment of process parameters, solar cells with optimized PV conversion efficiencies in excess of 8% can be achieved, with open-circuit voltages V_{OC} in the region of 500-550 mV [1].

As *SC* is varied either side of this optimum concentration there is a reduction in solar cell efficiency. In the more crystalline material deposited at low *SC*, this may be linked to an increase in spin density [2] arising from silicon dangling bonds at the crystalline column boundaries. Such bulk defects may be responsible for reduced cell performance [3]. It is believed that the column boundaries are passivated to some extent by the amorphous phase in mixed-phase material, leading to improved electronic properties. As *SC* is increased, the crystalline fraction continues to fall and the optical band-gap of the absorber and V_{OC} increase. Ultimately a point is reached where both the fill-factor *FF* and short-circuit current density J_{SC} decrease rapidly, and PV efficiency drops to as low as 2%. Further increase in *SC* yields nominally amorphous films containing no detectable crystalline volume fraction when analyzed by Raman spectroscopy, and the efficiency begins gradually to improve. By re-optimization of the deposition conditions in this regime good-quality solar cells may again be obtained, with V_{OC} now in the region 850-1000 mV [4]. Thus there are two regimes which, when approached from the microcrystalline and amorphous 'ends' of the silane : hydrogen dilution spectrum, may yield efficient solar cells, albeit with quite different spectral response, short-circuit current and open-circuit voltage.

Why solar cells with 'low-crystallinity' or 'Raman amorphous' absorber layers, lying between these two regimes, exhibit such poor PV performance forms the central question of this work. ESR studies [2] have shown that paramagnetic defects remain at a low level, and thus there is no reason to suspect an increase in defect-mediated recombination. It has been suggested that changes in growth conditions may instead give rise to local degradation of the *p-i* interface [5] and the formation of a space-charge which acts as a barrier to transport. This view is supported by the improved performance of cells containing buffer layers (see reference [6] for example), but these appear only to defer the decline in performance. More recently, time-of-flight (TOF) transport measurements [7, 10] have been carried out which indicate that in the low-crystallinity regime, both electron and hole bulk mobilities are significantly reduced relative to their values in optimized microcrystalline silicon films [11]. Indeed, the electron mobility appears even lower than in good-quality *amorphous* films. These variations in transport properties with composition were recently investigated by the present authors and their co-workers, by means of two-beam photogating measurements [12].

Here we consider two alternative modelling approaches to explain solar cell behaviour in the low-crystallinity region, each based on bulk, rather than interface, properties. The first may be termed an equivalent-circuit method. This is a more quantitative PSPICE [13] implementation of a proposal by the UniSolar group [14, 15] in which microcrystalline and amorphous phases in an inhomogeneous absorber layer are represented by two parallel-connected photodiodes, the photocurrent generation and diode transport parameters being scaled in proportion to the volume fraction of the constituents. This model was shown to predict *qualitatively* the observed increase in V_{OC} with increasing amorphous content, and with light-soaking, and is consistent with conductive AFM measurement of local current flows in mixed-phase material down to quite low volume fractions. We note that a similar approach comprising a mesh of discrete diode-resistor elements was proposed by the IPE Stuttgart group [16] to investigate the related issue of statistical fluctuations in homogeneity in a generalised solar cell. The second approach used here is based on solution of the transport equations, assuming multiple-trapping kinetics in a model density of states (DOS) consisting of exponential conduction and valence band tails and a Gaussian distribution of amphoteric dangling bond mid-gap defect states. Specifically, we investigate the influence of varying the electron and hole extended-state mobility, in keeping with the TOF results, on the solar cell parameters.

2. Experimental

2.1. Solar cell preparation

Cells were prepared in p-i-n sequence using a cluster-tool system, as described previously [17, 18]. The i-layer was deposited by PECVD at 20 W VHF power, at a rate of typically 0.3 - 1 nm/s onto a 10 cm × 10 cm glass substrate held at 200 °C. A series of depositions at *SC* between 5% and 15% were carried out, with nominal i-layer

thicknesses of 1 μm and 4 μm. The cells were completed by deposition of evaporated Ag back-contacts. In the case of the 4 μm series, one half of each substrate was prepared with millimeter dots of sputtered ZnO:Al, enabling illumination from either the p- or the n-side for TOF measurements. Raman spectroscopy (λ = 647 nm) was used to estimate film crystallinity. The integrated intensities of the phonon bands at 480 cm^{-1}, associated with disordered material, and at 505 and 518 cm^{-1}, associated with crystalline grains or columns, yield the Raman intensity ratio, $I_{CRS} = (I_{505} + I_{518})/(I_{480} + I_{505} + I_{518})$. Because the crystalline bands in low-crystallinity materials are small, to improve accuracy a background spectrum of amorphous silicon normalized to the 480 cm^{-1} band was subtracted prior to integration. Measurements with the laser incident from the film side and the glass side of the cell [7] were similar, indicating a fairly uniform composition in the direction of growth.

2.2. Equivalent-circuit model

The electrical model used to represent the mixed-phase solar cell is shown schematically in Fig. 1. The sources I_L represent the photocurrents generated by the microcrystalline and amorphous phases, denoted by the additional subscripts M and A respectively. Similarly, the components D, R_S and R_P embody charge transport through these phases between the top and bottom contacts. Lateral transport between phases is not included, and carrier transport paths through both phases are considered uniform. In this model therefore, the cross-sectional area is proportional to the volume of each phase, and is thus a scaling factor for each circuit element.

The starting point for the simulation requires the equivalent-circuit parameters for the limiting cases of 'fully microcrystalline' and 'fully amorphous' cells to be determined. However there is a problem if a '100% microcrystalline' cell is used to define the electrical parameters for the 'M' phase. It is well-known that very highly-crystalline cells ($I_{CRS} \geq 0.8$) have poor solar cell efficiencies (2-3%) and a low V_{OC} around 400 mV, associated with a high dangling-bond spin-density [19]. Increasing *SC* towards 6% yields progressively more efficient cells (~ 8%) and V_{OC} above 500 mV, prior to the onset of the rapid fall in efficiency described above. As mentioned above, these improvements are thought to result from passivation of unsatisfied bonds located at crystalline column boundaries by the amorphous material. This cannot be accounted for in the two-diode model since the optoelectronic 'quality' of the two components is inter-dependent. Therefore, we believe it is more appropriate to define the '100% M' limit as the optimum phase mixture of $I_{CRS} \sim 50\%$.

The volume fraction used in model scaling will be referred to simply as F. In scaling the 'M' parameters, the diode saturation current I_S is multiplied by F, the diode ideality factor N is unchanged, and the series and parallel resistances R_S and R_P are divided by F. The 'A' parameters are scaled similarly, but by the factor (1-F).

2.3. Transport model

Computer simulation of solar cells was carried out using the *SC-Simul* program developed at the University of Oldenburg. This is a one-dimensional numerical simulation which solves the Poisson equation, the continuity equations for electrons and holes, and the current transport equations including drift, diffusion, and thermionic emission over barriers, if present, in the valence and conduction bands. The thermal equilibrium and steady-state

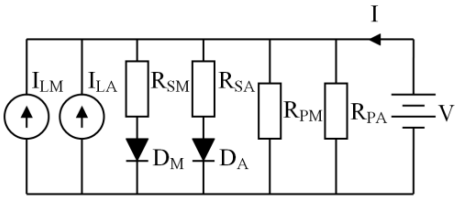

Fig. 1. Two diode equivalent-circuit model

Table 1. Two-diode equivalent-circuit model parameters (for 1 cm^2 cell area)

$d<i>$ (μm)	'M' phase				'A' phase			
	I_S (A)	N	R_S (Ω)	R_P (Ω)	I_S (A)	N	R_S (Ω)	R_P (Ω)
1	1.6E-08	1.5	1.0	1500	1.5E-10	1.8	4.0	800
4	4.5E-07	1.7	1.4	450	8.5E-07	3.0	5.0	350

solutions are obtained by Newton iteration. The semiconductor model is defined in terms of a device file which references material/optical absorption files appropriate for each layer of the device. For each material the DOS, capture coefficients, band mobilities etc. are defined. Further details are given in references [20] and [21].

3. Results and discussion

3.1. J-V characteristics – general features

The model parameters yielding best fits to the *J-V* characteristics at the fully microcrystalline and fully amorphous ends of the deposition range, for the 1 μm and 4 μm series, are listed in Table 1. Representative experimental (AM1.5) and simulated *J-V* characteristics over a range of material compositions for the 4 μm absorber layer series are shown in Figs. 2(a) and 2(b) respectively. It can be seen by comparing the sets of characteristics that the experimental trends are broadly reproduced by the two-diode model. However, it is not possible to make a detailed appraisal of the model from these characteristics alone. This may be carried out more thoroughly in terms of the solar cell parameters V_{OC}, J_{SC} and *FF*, which are routinely measured for a number of cells prepared simultaneously on the same substrate.

3.2. Relation between V_{OC} and I_{CRS}

One distinctive feature reported by many groups is the correlation between V_{OC} and I_{CRS}, illustrated in Fig. 3. The shape of this curve may be qualitatively understood in terms of the two-diode model as follows. Imagine we begin with a 'fully amorphous' cell, with its characteristic high V_{OC}, in the vicinity of 0.9 volts. Now consider the effect of a small amount of 'M' phase. Since D_M has a 'turn-on' voltage around 0.5 volts it becomes strongly forward-biased by the current generated primarily by the 'A' phase. Due to the exponential diode *J-V* relation, the

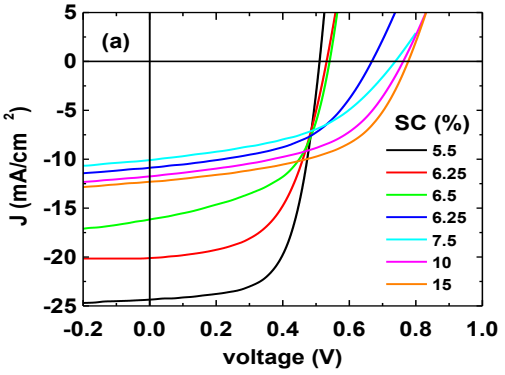

Fig. 2(a). Experimental *J-V* curves for cells deposited for *SC* between 5 and 15%. i-layer thickness in all cases nominally 4 μm.

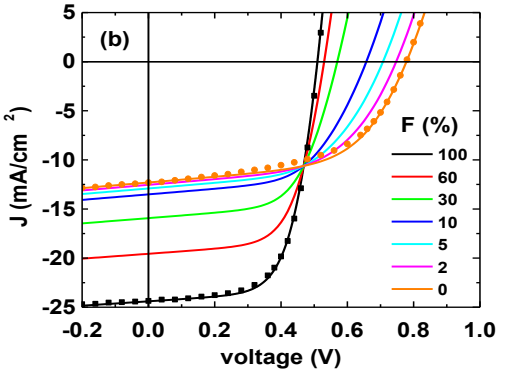

Fig. 2(b). Simulated *J-V* curves computed for *F* between 0 and 100%. Solid symbols are experimental data to which *F*=0 (circles) and *F*=100% (squares) curves were fitted.

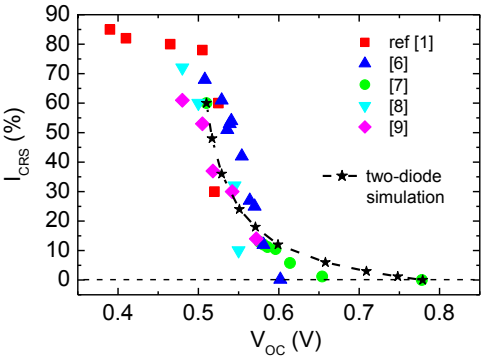

Fig. 3. Correlation between crystalline volume fraction and open-circuit voltage for several experimental studies (see references). Dashed line is simulated using two-diode model. F=100% is aligned with I_{CRS}=60%, as explained in the text.

$D_M + R_M$ series combination acts as a significant shunt across D_A. As the proportion of 'M' phase increases, the shunt effect increases and V_{OC} continues to fall, but less rapidly as V_{OC} approaches the 'turn-on' voltage of D_M.

With further increase in the 'M' phase, current is mostly generated by the 'M' phase and the 'A' phase plays a diminishing role in the cell characteristics as it neither conducts nor generates much current. As mentioned above, the 'A' phase is believed to improve the electrical quality of the 'M' phase by cloaking the dangling bonds and thereby reducing the defect density, but this cannot be included naturally in our model. It can be seen from Fig. 3 that the fit of the model curve to composite experimental data published by several groups is quite good, although it over-estimates somewhat the crystallinity of the 'Raman amorphous' material in the region $V_{OC} > 650$ mV.

As well as forming a test of the model, the correlation between V_{OC} and I_{CRS} is particularly useful because it justifies plotting other PV parameters versus V_{OC}, which is available for every cell, as a substitute for I_{CRS}, which would require extensive Raman measurements to be made, one at least per cell. Also, an absorber may show no discernible crystalline Raman peaks, yet systematic variations in J_{SC} and FF with V_{OC} may continue to occur [7]. Thus while it is accepted that the relationship between V_{OC} and I_{CRS} is not in general necessarily precise nor unique – for example, V_{OC} is slightly reduced in thicker cells [22] – for our purposes it forms a convenient parameter through which to compare the two-diode model with experiment, as we present below.

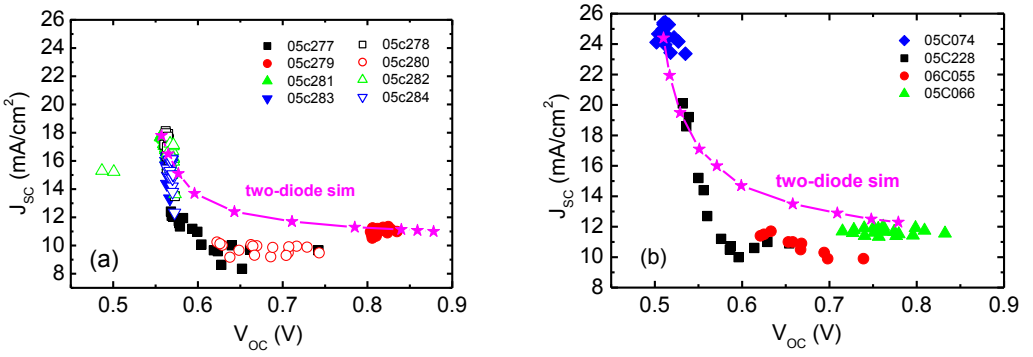

Fig. 4. Measured variation of short-circuit current density with open-circuit voltage for cells prepared over a range of *SC*, and corresponding simulations using the two-diode model. Nominal i-layer thicknesses 1 μm in (a), and 4 μm in (b).

3.3. Relation between J_{SC} and V_{OC}

We now consider whether the two-diode model can correctly reproduce the behaviour of J_{SC} in the low-crystallinity region. Figs. 4(a) and 4(b) illustrate this for the 1 µm and 4 µm series, respectively. The experimental data show a rapid fall in J_{SC} with increasing V_{OC} in both cases, which then plateaus out. The simulation reproduces to some extent the observed fall in current on approaching the low-crystalline regime, suggesting that a linear superposition of the currents generated by the microcrystalline and amorphous fractions is a realistic assumption. However, the experimental relationship falls somewhat more steeply, and reaches a plateau which lies below the model prediction. This may be an indication of additional carrier loss due to increased recombination in the low-crystallinity material, which is not included in this model.

Considerable variation in solar cell parameters across the substrate occurs within each deposition. Under the growth conditions used in the present work, material deposited on the central region of the substrate is more crystalline than at the edges, and this typically yields cells with lower V_{OC}, as is explored in more detail in reference [7]. This is a beneficial side-effect in this study, since each single deposition on to a 10 × 10 cm glass substrate can provide up to eighteen 1 × 1 cm^2 cells of intermediate crystallinity. Yan *et al* [15] report a similar effect, but in their case the central region of the substrate appears more amorphous.

3.4. Relation between FF and V_{OC}

Figs. 5(a) and 5(b) show the experimental and model variations in *FF* with crystallinity. For the 1 µm film, the pattern of change is quite well reproduced, though the experimental *FF* values lie somewhat below the predicted values. For the 4 µm film, the strong dip in the experimental *FF*, from 65% to below 40%, is not reproduced by the model. The simulation predicts a minimum in *FF*, but it is in the wrong position and is also far too shallow. As discussed above, the reason for the minimum in *FF* in the two-diode model is the loss of current available to an external load due to the internal shunting effect of the microcrystalline phase. This appears insufficient to explain the experimental results. Given that the 4 µm absorber is more strongly in disagreement, one might suggest that the poor performance of low-crystallinity absorber material has its origins in a bulk, rather than a surface, effect.

3.5. Relation between PV conversion efficiency and V_{OC}

Figs. 6(a) and 6(b) compare the experimental and simulated efficiencies. While the simulation bears the correct general shape, it is not in good quantitative agreement with experiment. This is not surprising, given the efficiency relies upon the correct treatment of the other PV parameters, for which there are a number of discrepancies as discussed above.

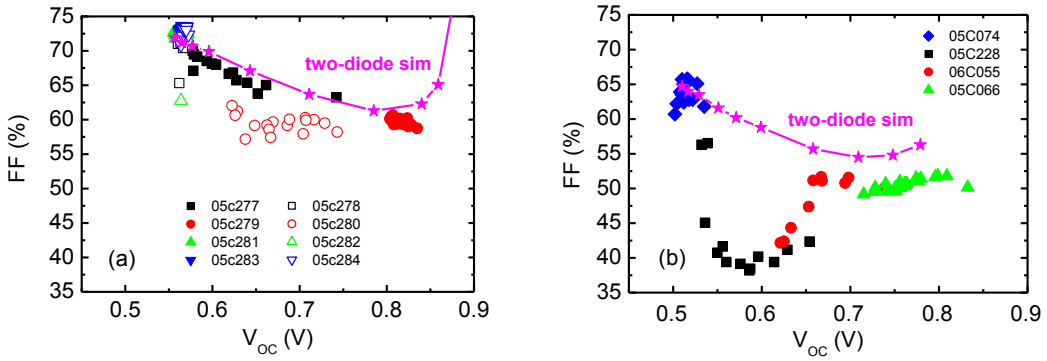

Fig. 5. Measured variation in fill-factor with open-circuit voltage for solar cells prepared over a range of *SC*, and the corresponding simulations using the two-diode model. Nominal i-layer thicknesses 1 µm in (a), and 4 µm in (b).

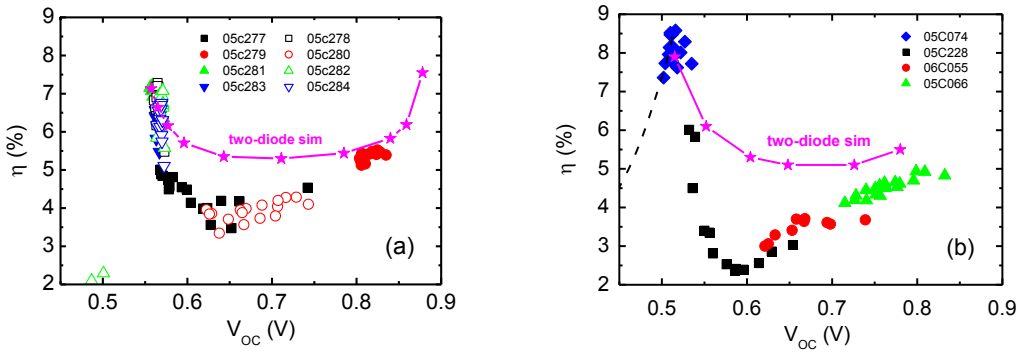

Fig. 6. Measured variation in conversion efficiency for solar cells prepared over a range of *SC*, plotted vs. V_{OC}, and the corresponding simulations using the two-diode model. The nominal i-layer thicknesses were 1 μm in (a), and 4 μm in (b).

3.6. Transport simulation – mobility model

As previously discussed, microcrystalline silicon is a mixed-phase material whose structure, composition and optoelectronic properties are strongly influenced by deposition conditions. The two-diode model assumes that it is possible to separate the microcrystalline and amorphous phases into a lumped equivalent circuit, and then to apply a mixing coefficient '*F*' which enables the constituents to be reassembled in the appropriate proportions. We have seen that this model is successful in certain respects, and less so in others. The transport simulation approach, however, views the p, i and n layers as homogeneous and assigns effective physical parameters to them, as listed in Table 2. This procedure requires further elaboration.

It is generally accepted that microcrystalline silicon has an 'energy gap' which may vary, depending on composition, between 1.1 eV (the silicon crystal indirect gap) and 1.8 eV (the nominal value for amorphous silicon). This is expected to result in an increase in V_{OC} and a decrease in J_{SC} in moving from more crystalline to more amorphous cell deposition conditions. However there is no obvious reason why this should give rise to the poor *transport* properties of low-crystalline material, as evidenced by the low fill-factor. To simplify matters in our simulations we assume a fixed mobility gap of 1.3 eV, and a fixed absorption spectrum, similar to that of the optimum phase mixture, independent of composition.

Our model approach combines the microscopic effects on transport associated with changes in composition into the lumped parameter 'mobility'. The motivation for doing so is that the TOF mobility [10, 11] appears to follow these changes, as shown in Fig. 7. A speculative picture of the electronic energy landscape in microcrystalline silicon is shown in Fig. 8. We envisage that the total density of states is composed of an admixture of states associated with amorphous silicon, namely extended (transport) states, localised band tail states, and dangling bond defects in mid-gap, and with crystal silicon, which furnishes conduction and valence band states. When the

Table 2. Absorber layer model parameters used in solar cell simulation

E_G (eV)	μ_{0e} (cm^2/(Vs))	μ_{0h} (cm^2/(Vs))	N_C (cm^{-3})	N_V (cm^{-3})	kT_C (eV) [1]	kT_V (eV) [1]	E_D (eV)	N_D (cm^{-3}) [2]	U (eV)
1.3	varied	varied	10^{20}	10^{20}	0.02	0.035	0.7	3×10^{15}	0.2

Key: E_G energy bandgap; μ_{0e} free electron mobility; μ_{0h} free hole mobility; N_C effective density of CB states; N_V effective density of VB states; kT_C CB tail slope; kT_V VB tail slope; E_D defect peak energy; N_D defect density; U correlation energy. All energies measured relative to $E_V = 0$. Simulation temperature $T = 300$ K throughout.

[1] Electron and hole capture coefficients into CB and VB tail states: 10^{-9} cm^3s^{-1}

[2] Electron and hole capture coefficients into (i) neutral defects: 5×10^{-9} cm^3s^{-1}, (ii) charged defects: 5×10^{-8} cm^3s^{-1}

p-layer: thickness 30 nm, Fermi-level 0.2 eV; n-layer: thickness 30 nm, Fermi-level 1.1 eV.

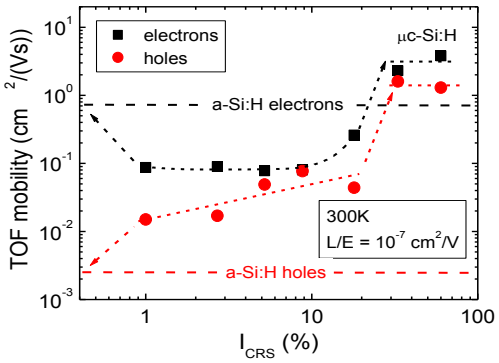

Fig. 7. Variation in electron and hole TOF mobility vs. crystalline volume fraction, after reference [10].

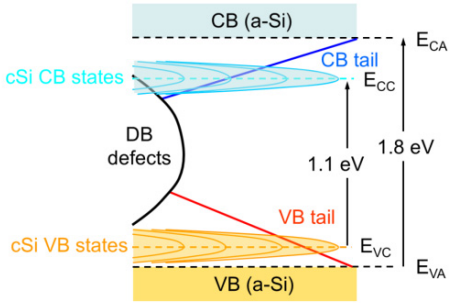

Fig. 8. Proposed density of states landscape in low-crystalline microcrystalline silicon.

crystalline fraction is high, transport proceeds via these states. Frequent scattering in the band states reduces mobility to well below single-crystal values (1 to 100 $cm^2/(Vs)$). The structural disorder associated with grain boundaries plus amorphous material [23, 24] contributes localised tail states which capture free carriers and slow their progress via multiple-trapping [25], but the mobility of both electrons and holes is enhanced over amorphous silicon by virtue of the faster band transport. As the crystalline content is reduced (silane concentration in the process gas increased) enhanced mobility persists until the crystalline states are no longer sufficiently overlapped. At this point, these states become localised in character, and essentially add to the density of shallow trap states, superimposed on the band tails. This reduces the electron mobility significantly, to below the value in amorphous silicon. For holes the mobility also falls, but it remains above the much lower value in amorphous silicon. Further increase in silane concentration deposits material having the properties of amorphous silicon. Higher hole mobility has also been reported in amorphous silicon deposited by the expanding thermal plasma technique [26], which is thought to be due to enhanced medium-range order in the amorphous phase resulting in a steeper valence band tail.

This picture envisages radical and complex changes in the density of states. Rather than attempt in a simulation to implement these in detail by introducing changes in band tail densities and slopes, capture properties, band offsets etc. we have maintained the localised DOS profile associated with the optimum phase material throughout, and simply varied the extended state mobilities for electrons and holes. In line with the TOF mobility data, we fix the electron to hole mobility ratio to be a factor of three, and treat this as the variable parameter in our simulations.

The effect on fill-factor for a 1 μm and a 4 μm cell is shown in Fig. 9, simulated under AM1.5 conditions. Both cells show a reduction in *FF* with decreasing mobility values, but the thicker cell is more strongly affected. The bars marked 'OPM' and 'L-C' correspond to the *FF* values measured in cells deposited in the optimum phase mixture and low crystalline regimes, respectively. With reference to Figs. 5(a) and 5(b) we see that the model correctly predicts the size of the reduction in *FF* for a 1 μm cell (from around 70% to 60%) and for a 4 μm cell (from 65% to 40%). We have also simulated the spectral dependence of short-circuit current, to construct the quantum efficiency curves parametric in mobility for a 4 μm cell, shown in Fig. 10. These predict a strong reduction in *QE* in the blue-green part of the spectrum in passing from OPM to L-C regimes, by around a factor of 20. The reduction in the red part of the spectrum is a factor of 2 or less. This is in good agreement with the experimental data shown in Fig. 11, where the short-circuit currents recorded in filtered AM1.5 are plotted against V_{OC} which, to enable a consistent comparison to be made, is the value measured under un-filtered AM1.5. The experimental measurement of photo-response will also be subject to changes in optical absorption coefficients, particularly in the red/IR region of the spectrum, as discussed above. Overall then, by adjusting the extended-state mobility in the transport simulation it is possible to reproduce certain experimental features associated with optimum phase mixture and low-crystalline thin-film silicon solar cells.

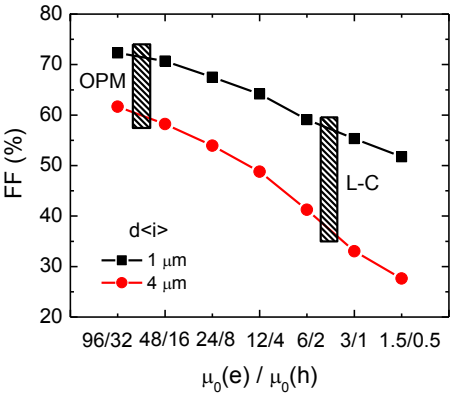

Fig. 9. Simulated dependence of fill-factor with mobility fraction for 1 μm and 4 μm absorber layers. OPM and L-C denote the measured fill-factors for optimum phase mixture and low-crystalline films, respectively.

4. Conclusions

A simple two-diode equivalent-circuit model of a mixed-phase microcrystalline silicon *pin* solar cell has been evaluated with regard to its ability to reproduce the PV parameters of experimentally-measured test cells prepared in the low-crystalline content absorber region. It is demonstrated that this model is able to reproduce quite well the relationship between open-circuit voltage and crystalline content of the absorber layer. It is proposed that the open-circuit voltage may thus be used as a means of estimating crystalline content in the cell series studied here. Within the two-diode model, the short-circuit current is a simple addition of the currents generated by the amorphous and crystalline fractions. While there are some discrepancies in detail, the general features in a plot of short-circuit current versus open-circuit voltage measured over a range of crystallinities are fitted quite well by this model, although generally the short-circuit currents in the low-crystallinity absorber region are lower than predicted by the model. The fill-factor is predicted to decrease in this region, but the dip observed experimentally for a thick absorber is far larger than the model indicates. A lack of quantitative agreement suggests that this simple model is

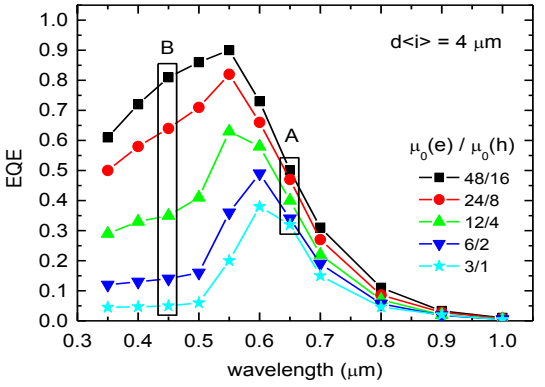

Fig. 10. Simulated quantum efficiency curves for several mobility fractions. Regions A and B correspond approximately to illumination conditions under which measurements in Fig. 11 were taken.

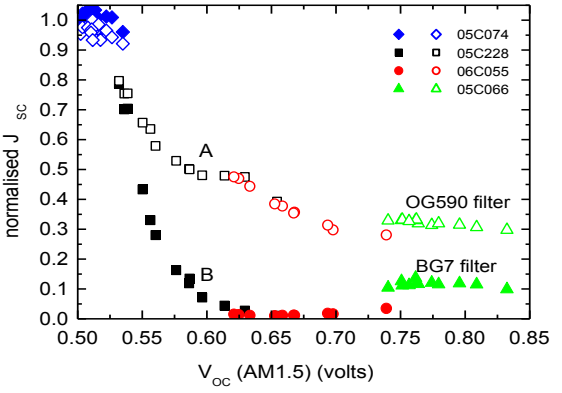

Fig. 11. Normalised short-circuit current vs. V_{OC} for 4 μm absorber layer cells. AM1.5 illumination through long-pass 590 nm filter (OG590, curve A, open symbols) and blue-green (370-550 nm) bandpass filter (BG7, curve B, filled symbols).

somewhat incomplete. This may be because it over-simplifies the system, for example by not including lateral interactions between absorber layer regions.

Electrical power dissipation due to internal shunting by more highly-crystalline material, at least in the manner embodied in the two-diode model, may therefore be insufficient to account for the observed behaviour in detail. Bearing in mind that there is no evidence for an increased bulk density of defects in low-crystalline material, we have investigated the possible consequences of variations in carrier mobilities measured by time-of-flight experiments. By introducing changes in band mobility into a transport model of the solar cell, in proportion to the observed variations in time-of-flight mobility, we are able to reproduce the magnitude of the dip in fill-factor, the larger dip in cells with a thicker absorber layer, and the observed spectral dependence in quantum efficiency.

A tentative density of states picture has been proposed to account for variations in mobility with composition. In the optimum phase mixture, the crystalline states participate as high-mobility transport states. In low-crystalline material they contribute additional shallow localized states which have a deleterious effect on mobility since they act as carrier traps and reduce the fraction of free carriers in extended states.

Acknowledgements

The authors are grateful for the assistance of Y. Mai in depositing the cells investigated in this study, to W. Reetz for *J-V* measurements, and to M. Hülsbeck for Raman characterizations.

References

[1] Vetterl O, Finger F, Carius R, Hapke P, Houben L, Kluth O, Lambertz A, Mück A, Rech B, Wagner H. Intrinsic microcrystalline silicon: A new material for photovoltaics. *Sol Energy Mater Sol Cells* 2000; **62**:97.

[2] Astakhov O, Carius R, Finger F, Petrusenko Y, Borysenko V, Barankov D. Relationship between defect density and charge carrier transport in amorphous and microcrystalline silicon. *Phys Rev B* 2009;**79**:104205.

[3] Smirnov V, Astakhov O, Carius R, Pieters BE, Petrusenko Y, Borysenko V, Finger F. Performance of p- and n-side illuminated microcrystalline silicon solar cells following 2 MeV electron bombardment. *Appl Phys Lett* 2012;**101**:143903.

[4] Myong S, Sriprapha K, Yashiki Y, Miyajima S, Yamada A, Konagai M. Silicon based thin-film solar cells fabricated near the phase boundary by VHF PECVD technique. *Sol Energy Mater Sol Cells* 2008;**92**:639-645.

[5] Stiebig H, Brammer T, Zimmer J, Vetterl O, Wagner H. Investigation of the optoelectronic properties of μc-Si:H pin solar cells. *J Non-Cryst Solids* 2000;**266-269**:1104-1108.

[6] Mai Y, Klein S, Carius R, Stiebig H, Geng X, Finger F. Open circuit voltage improvement of high-deposition-rate microcrystalline silicon solar cells by hot wire interface layers. *Appl Phys Lett* 2005;**87**:073503.

[7] Reynolds S, Carius R, Finger F, Smirnov V. Correlation of structural and optoelectronic properties of thin film silicon prepared at the transition from microcrystalline to amorphous growth. *Thin Solid Films* 2009;**517**:6392-6395.

[8] Lambertz A, Finger F, Carius R. Silicon solar cells and material near the transition from microcrystalline to amorphous growth. *Proceedings of 3rd World Conference on Photovoltaic Energy Conversion* (Osaka, May 11-18 2003), Vols. A-C, p. 2738.

[9] Bailat J, Poruba A, Mullerova L, Springer J, Vanecek M, Vallat-Sauvain E, Meillaud F, Niquille X, Dubey M *et al.* Active layer quality and open-circuit voltage of nip and pin microcrystalline solar cells. *Proceedings of the 19th European PV Solar Energy Conference* (Paris, June 2004), p. 1541-1544.

[10] Reynolds S. Carrier mobility, band tails and defects in microcrystalline silicon. *J Phys Conf Ser* 2010;**253**:012002.

[11] Dylla T, Reynolds S, Carius R, Finger F. Electron and hole transport in microcrystalline silicon solar cells studied by time-of-flight photocurrent spectroscopy. *J Non-Cryst Solids* 2006;**352**:1093.

[12] Reynolds S, Main C, Smirnov V, Meftah A. Intensity dependence of quantum efficiency and photo-gating effects in thin film silicon solar cells. *Phys Status Solidi (c)* 2010;**7**:505.

[13] Castaner L, Silvestre S. *Modelling Photovoltaic Systems using PSpice*. Chichester: Wiley; 2002.

[14] Yan B, Yang J, Yue G, Lord K, Guha S. On the mechanism of light-induced open-circuit voltage increase in mixed-phase hydrogenated silicon solar cells. *Proceedings of 3rd World Conference on Photovoltaic Energy Conversion* (Osaka, May 11-18 2003), Vols. A-C, p. 1627-1630.

[15] Yan B, Jiang C, Teplin C, Moutinho H, Al-Jassim M, Yang J, Guha S. Local current flow in amorphous and nanocrystalline mixed-phase silicon solar cells. *J Appl Phys* 2007;**101**:033712.

[16] Grabitz PO, Rau U, Werner JH. Modeling of spatially inhomogeneous solar cells by a multi-diode approach. *Phys Status Solidi (a)* 2005;**202**:2920.

[17] Mai Y, Klein S, Carius R, Wolff J, Lambertz A, Finger F, Geng X. Microcrystalline silicon solar cells deposited at high rates. *J Appl Phys* 2005;**97**:114913.

[18] Gordijn A, Pollet-Villard A, Finger F. At the limit of total silane gas utilization for preparation of high-quality microcrystalline silicon solar cells at high-rate plasma deposition. *Appl Phys Lett* 2011;**98**:211501.

[19] Baia Neto A, Lambertz A, Carius R, Finger F. Relationships between structure, spin density and electronic transport in 'solar-grade' microcrystalline silicon films. *J Non-Cryst Solids* 2002;**299-302**:274.

[20] Rösch M. PhD thesis, University of Oldenburg (2003) (in German). Available at http://oops.uni-oldenburg.de/247/2/roeexp03.pdf
The SC-Simul software may be downloaded from: http://www.greco.uni-oldenburg.de/26446.html.
[21] Brüggemann R, Rösch M. Application of SC-Simul – Numerical simulation for thin-film silicon based devices. *J Optoel Adv Mater* 2005;**7**:65-72.
[22] Gross A, Vetterl O, Lambertz A, Finger F, Wagner H, Dasgupta A. N-side illuminated microcrystalline silicon solar cells. *Appl Phys Lett* 2001;**79**:2841.
[23] Kočka J, Fejfar A, Stuchlíková H, Stuchlík J, Fojtík P, Mates T, Rezek B, Švrček V, Pelant I. Basic features of transport in microcrystalline silicon. *Sol Energy Mater Sol Cells* 2003;**78**:493.
[24] Reynolds S, Smirnov V, Finger F, Main C, Carius R. Transport and Instabilities in Microcrystalline Silicon Films. *J Optoel Adv Mater* 2005;**7**;91-98.
[25] Tiedje T. Time-resolved charge transport in hydrogenated amorphous silicon. *The Physics of Hydrogenated Amorphous Silicon II. Topics in Applied Physics* 1984;**56**:261-300.
[26] Brinza M, Emelianova EV, Adriaenssens GJ. Nonexponential distributions of tail states in hydrogenated amorphous silicon. *Phys Rev B* 2005;**71**:115209.